Sensitivity enhancement of a wavelength interrogation-based optical fiber surface plasmon resonance sensor for hemoglobin concentration using barium titanate

ZHEN-JIANG SHI[1,2,3], SHI-LIANG GUO[1,2,*], XIN LI[4], ZHI-QUAN LI[1,2],
SHU-HAN MENG[1,2], CHONG-ZHEN LI[1,2]

[1]Engineering Research Center of the Ministry of Education for Intelligent Control System
 and Intelligent Equipment, Yanshan University, Qinhuangdao, China, 066000

[2]Key Laboratory of Industrial Computer Control Engineering of Hebei Province,
 Yanshan University, Qinhuangdao, China, 066000

[3]Department of Engineering Technology, Open University of Guangdong
 (Guangdong Polytechnic Institute), Guangzhou, China, 510091

[4]School of Mathematics and Information Technology, Hebei Normal University of Science
 and Technology, Qinhuangdao, China, 066000

In this paper, the performances of a wavelength interrogation-based optical fiber surface plasmon resonance sensor for hemoglobin (Hb) concentration is investigated by theoretical simulation. The proposed configuration incorporates optical fiber, 70 nm silver, 18 nm barium titanate ($BaTiO_3$), and 2 nm zinc oxide. Simulation results show the sensor exhibits refractive index sensitivity of 4023 nm/RIU and concentration sensitivity of 10.0873 nm/(g·dL), along with Hb concentration varying from 0 to 14 g/dL. This paper especially focuses on the influence of $BaTiO_3$ on the performances of the proposed sensor with light wavelength ranging from 350 to 1000 nm. Comparison analysis indicates sandwiching 18 nm $BaTiO_3$ between sensing layers not only enhances the concentration sensitivity by 30.14% but also decreases the nonlinear error of the sensor from 0.68% to 0.63%. For a wavelength accuracy of 0.1 nm, the proposed sensor can provide a resolution of 0.0099 g/dL for Hb concentration detection.

Keywords: surface plasmon resonance, wavelength interrogation, barium titanate, sensitivity enhancement, hemoglobin concentration.

1. Introduction

Hemoglobin (Hb) is a critical globular heme protein in the human body, and its content is an important physiological index to reflect whether the human body suffers from

blood diseases such as anemia. Therefore, the sensing and detection technique for Hb concentration plays an important role in the evaluation of human health [1]. Concentration-dependent Hb refractive index (RI) in the wavelength range from 250 to 1100 nm using model function was calculated [2], and the RI data of human Hb in the visible range were detailed in [3]. At any wavelength, the RI of a blood sample varies linearly with the Hb concentration [4]. Therefore, the Hb concentration can be obtained by measuring the RI.

Surface plasmon resonance (SPR) is a widely used plasmonic based optical sensing technique for identifying minute variation in the RI of a measured sample adjacent to the metal surface. Hence, accurate detection for the concentration of an Hb sample can be realized by utilizing an SPR sensor [5]. It is an invasive detection approach for Hb concentration and can provide quick, label-free, and real-time detection with a high sensitivity [6]. Plasmonic-based biosensing was first explored by Liedberg *et al*. [7]. Brahmachari and Ray investigated the effect of light coupling prism materials on plasmonic biosensing for detecting wavelength and concentration dependent RI variations of oxygenated native Hb solution from 700 to 900 nm wavelength in the near infrared region [8]. Heidarzadeh utilized different shapes of silver (Ag) plasmonic nanoparticles for the detection of Hb concentration of 140 g/L [9]. Mohanty and Sahoo theoretically investigated the effect of III–V nitride semiconductors on the overall sensitivity and resolution of a graphene-based SPR biosensor for the measurement of Hb concentration in a human blood sample [10]. However, the existing literature mostly used prism-based sensor and adjusted the incident angle of a fixed wavelength light to excite SPR, which is not convenient for applications.

Now, optical fiber is used instead of prism, metal, and other nanomaterials as well as tunable laser light source to excite SPR in wavelength interrogation mode. Thus far, optical fiber-based SPR sensor has been demonstrated both experimentally and theoretically in many research studies [11–16]. Compared with the prism-based Kretschmann configuration, the optical fiber-based SPR sensor provides several benefits such as simplified, flexible optical design, convenience for remote sensing, continuous analysis, and *in situ* monitoring [17–19]. Sharma proposed a fused silica substrate-based SPR sensor for the detection of Hb concentration in human blood using angular interrogation [20]. Luo and Wang utilized an optical fiber-based SPR sensor modified with gold (Au) film and carbon nanotubes for measuring the concentration of dissolved oxygen in Hb and obtained the detection sensitivity of 8.89 nm/(mg/L) [21].

In this investigation, an optical fiber-based SPR sensor is proposed based on a silver (Ag)/barium titanate ($BaTiO_3$)/zinc oxide (ZnO) sandwiched structure to measure the Hb concentration using wavelength interrogation. This paper focuses on the parameter optimization of the sensing layers, especially the enhancement sensitivity by using $BaTiO_3$. Section 2 demonstrates the material and mechanism of the proposed sensor. Section 3 discusses the theoretical analysis of the proposed configuration. Sections 4 and 5 consist of results, discussion, and conclusion of the proposed work.

2. Material and mechanism

The property of a nanomaterial has a remarkable influence on the performance of optical fiber-based SPR sensor. Therefore, how to select the nanomaterial of sensing structure to improve the performance has become a research hotspot in the application for optical fiber-based SPR sensor [22,23]. In this section, our proposed structure for Hb concentration detection is gradually developed.

The proposed multi-layered structure is shown in Fig. 1. The cladding of optical fiber is removed from a small part of the optical fiber, and the unclad core is subsequently coated with Ag, $BaTiO_3$, and ZnO nanolayer.

Silver (Ag) and gold (Au) are normally used as metal materials for plasmonic sensor. The SPR sensor using Ag material as sensing layer has a higher figure of merit (FOM) and detection accuracy (DA) than Au material, so Ag is utilized as metal nanomaterial adjacent to optical fiber surface. Among the common 2D nanomaterials, $BaTiO_3$ is a material with a high real part of RI and without any imaginary part. $BaTiO_3$ film is helpful for improving the sensitivity of the sensor for its high real part of RI. SUN *et al*. reported a prism-based SPR sensor decorated with 45 nm Ag film, 10 nm $BaTiO_3$ thin film, and monolayer graphene, and incorporating $BaTiO_3$ film provides a considerable shift in the SPR curve with a slight rise in the sensing layers RI [24]. In addition, WANG *et al*. reported an optical fiber SPR sensor decorated with 50 nm thick Au film and 10 nm thick $BaTiO_3$ thin film; the experimental results showed that the sensitivity of optical fiber/Au film/$BaTiO_3$ film SPR sensor was 25% higher than that of traditional Au film SPR sensor [25]. In addition, the imaginary part of $BaTiO_3$'s RI is 0, so the $BaTiO_3$ film does not attenuate the optical signal. Therefore, $BaTiO_3$ material was selected to enhance the sensitivity of the SPR sensor, and the $BaTiO_3$ film was covered on the Ag film. ZnO is one of the most important transition metal oxides with good optical properties [26]. It is a wide-band-gap semiconductor with a band gap of about 3.37 eV at 300 K. In addition, due to the large defects and oxygen vacancies, ZnO is suitable for biosensors, gas sensors, and chemical sensors [27,28]. These defects increase the
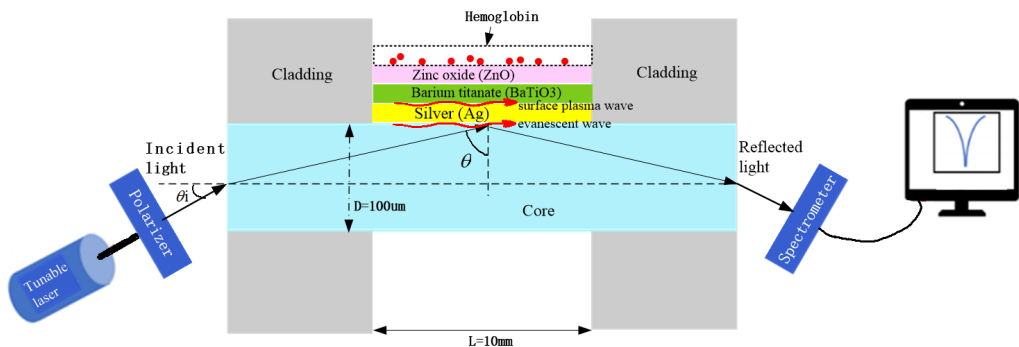

Fig. 1. Schematic diagram of proposed optical fiber-based SPR sensor.

interaction of ZnO with the analyte, resulting in better sensing. The use of ZnO layer can enhance the sensitivity of optical fiber-based SPR sensor due to high dielectric constant of ZnO [29], and the ZnO layer is extremely suitable for protecting other layers against oxidation [30]. Therefore, ZnO was used as the outermost layer adjacent to the Hb sample in the multi-layered structure.

Figure 1 shows the incident p-polarized light from a tunable laser light source is emitted into one end of the optical fiber, and the reflected light is recorded by the spectrometer at the other end of the optical fiber. The different-wavelength lights from the tunable laser light source are incident into the fiber core at a fixed angle θ_i. After multiple reflections at the interface between the core and the cladding, they reach the interface between the core and the metal at the angle θ required to cause SPR, which was assumed as 85° in this paper and used to determine the value of θ_i. When the wave vector of the evanescent wave matches the wave vector of the surface plasmon wave, the surface plasmon is excited and a sharp drop in the reflected spectrum is obtained at a specific wavelength called resonance wavelength, which relates to the RI of Hb sample and the thicknesses of sensing layers-Ag, BaTiO$_3$, and ZnO. Keeping the thicknesses of sensing layers unchanged, a variation in the RI of Hb sample can be measured by identifying resonance wavelength shift.

3. Mathematical framework

In the proposed optical fiber-based SPR sensor, the prism is replaced by the core of the optical fiber, which is made of fused silica (numerical aperture NA = 0.24, core diameter $D = 100$ μm), and its RI dispersion relation is as follows:

$$n_{\text{core}}(\lambda) = \sqrt{1 + \frac{a_1 \lambda^2}{\lambda^2 - b_1^2} + \frac{a_2 \lambda^2}{\lambda^2 - b_2^2} + \frac{a_3 \lambda^2}{\lambda^2 - b_3^2}} \tag{1}$$

where λ is the wavelength of the incident light (μm); $a_1 = 0.6961663$, $a_2 = 0.4079426$, $a_3 = 0.8974794$, $b_1 = 0.0684043$ μm, $b_2 = 0.1162414$ μm, and $b_3 = 9.896161$ μm are the Sellmeier coefficients [31].

According to the Drude model, the RI dispersion relation of Ag can be written as

$$n_{\text{Ag}}(\lambda) = \sqrt{\frac{1 - \lambda^2 \lambda_c}{\lambda_p^2 (\lambda_c + i\lambda)}} \tag{2}$$

where $\lambda_p = 1.4541 \times 10^{-7}$ m and $\lambda_c = 1.7614 \times 10^{-5}$ m are the plasma wavelength and the collision wavelength of Ag, respectively [32].

According to the Sellmeier equation [33], BaTiO$_3$ has the RI dispersion relation that can be written as

$$n_{\text{BaTiO3}}(\lambda) = \sqrt{1 + \frac{4.187}{1 - (0.223/\lambda)^2}} \tag{3}$$

In terms of the Drude model [34], the RI dispersion relation of ZnO can be written as

$$n_{\text{ZnO}}(\omega) = \sqrt{\varepsilon_{\infty} - \left(\frac{\omega_p^2}{\omega^2 + \gamma^2} + i \frac{\gamma \omega_p^2}{\omega(\omega^2 + \gamma^2)} \right)} \tag{4}$$

where $\omega = 2\pi C/\lambda$, C is the speed of light in vacuum, $\varepsilon_{\infty} = 3.40$ is the high-frequency dielectric constant, $\omega_p = 2 \times 10^{15}$ Hz is the plasma frequency, and $\gamma = 1.5 \times 10^{14}$ Hz is the damping frequency [35].

The RI of Hb sample is given as

$$n_{\text{Hb}}(\lambda) = n_{\text{H2O}}(\lambda)(\beta C_{\text{Hb}} + 1) \tag{5}$$

where $\beta = 0.00199$ dL/g is the mean constant specific refractive increment of Hb for the wavelength range of 310–355 and 500–1100 nm [2], C_{Hb} denotes the concentration of Hb, and $n_{\text{H2O}}(\lambda)$ is the RI dispersion equation of water, referring to the formula in the literature [36].

In this paper, the following assumptions and simplifications are made on the theoretical model of optical fiber SPR sensor: only the case of light-excited SPR on the meridional plane is considered; the propagation mode of the incident light in the fiber is continuous; the range of incident angles is greater than the critical angle to an angle of 90°. Through the above assumptions, five-layer dielectric plane SPR theory can be used to analyze the sensing characteristics of the transmissive fiber SPR [25]. The proposed sensor was numerically calculated based on the principle of N-layer reflection method.

Fresnel multilayer reflection formula was applied for the N-layer model to calculate the reflectance coefficient r defined as

$$r = \frac{r_{\text{core\_to\_Ag}} + r_{\text{Ag\_to\_Hb}} \exp(2ik_{\text{Ag}}d_{\text{Ag}})}{1 + r_{\text{core\_to\_Ag}} r_{\text{Ag\_to\_Hb}} \exp(2ik_{\text{Ag}}d_{\text{Ag}})} \tag{6}$$

where $r_{\text{core\_to\_Ag}}$ is the reflection coefficient of the interface between the optical fiber core and the Ag layer, $r_{\text{Ag\_to\_Hb}}$ is the reflection coefficient related to n_{BaTiO3}, n_{ZnO}, and n_{Hb}, $k_{\text{Ag}} = (2\pi/\lambda)n_{\text{Ag}}\sin\theta$ is the wave vector in Ag film, and d_{Ag} is the thickness of Ag film.

While the reflectance R, defined as $|r|^2$, obtains the minimum for a RI of an Hb sample, it means SPR takes place and the resonance wavelength λ_{res} satisfies the following equation

$$\frac{2\pi}{\lambda_{\text{res}}} n_{\text{core}}(\lambda_{\text{res}}) \sin\theta = \text{real}\left\{ \frac{2\pi}{\lambda_{\text{res}}} n_{\text{sp}}(\lambda_{\text{res}}) \right\} \tag{7}$$

where θ is the angle between light and the interface normal of fiber core and metal layer and is assumed 85° in this paper, $n_{\text{core}}(\lambda_{\text{res}})$ is the RI of optical fiber core, and $n_{\text{sp}}(\lambda_{\text{res}})$ is the effective RI incorporating n_{Ag}, n_{BaTiO3}, n_{ZnO}, and n_{Hb}.

Hence, a minute variation of Hb concentration ΔC_{Hb} leads to the corresponding variation of RI Δn_{Hb} and in turn, the shift in resonance wavelength $\Delta\lambda_{res}$ of SPR reflected spectrum, with reflectance R reaching a minimum. Thus, the sensitivity for Hb concentration and RI can be represented as $S_C = \Delta\lambda_{res}/\Delta C_{Hb}$ (nm/(g·dL)) and $S_n = \Delta\lambda_{res}/\Delta n_{Hb}$ (nm/RIU), respectively, which are the most important performances of SPR sensor.

Full width at half maximum (FWHM) represents the width of the SPR curve, where the reflectivity is 50% of the maximum value. FWHM should be as low as possible to obtain sharp and narrow SPR curve, and high DA of the sensor, which can be expressed as DA = 1/FWHM.

In addition to sensitivity S, FOM is a critical performance of the SPR sensor and should be as high as possible, which can be calculated by FOM = S/FWHM [37]. Therefore, FOM is preferred for the overall performance of the sensor, as it includes both FWHM and sensitivity.

4. Results and discussion

4.1. Performance optimization

The performance of the Hb concentration sensor proposed with sensing layer thicknesses is optimized in this section to balance the photon absorption energy efficiency and energy loss of each layer [23]. FWHM, sensitivity, reflectivity, and FOM are used to optimize the parameters along with the light wavelength of 350–1000 nm, which is limited by the dispersion property of BaTiO$_3$ RI [33]. The concentration of Hb sample ranges from 0 to14 g/dL, and the corresponding RI varies from 1.33 to 1.36 RIU [38].

Different from angular interrogation, FWHM is an important parameter in wavelength interrogation mode for identifying the integrity and effectiveness of the reflected SPR spectrum. Figure 2 shows the variation of FWHM with 20, 30, 40, 50, 60, 70, 80, and 90 nm thick Ag along with BaTiO$_3$ thickness from 2 to 20 nm with interval of 2 nm, ZnO thickness from 2 to 12 nm with interval of 2 nm, and Hb concentration of 14 g/dL. In Fig. 2, d_{Ag}, d_{BaTiO3}, and d_{ZnO} denote the thickness of Ag, BaTiO$_3$, and ZnO, respec-
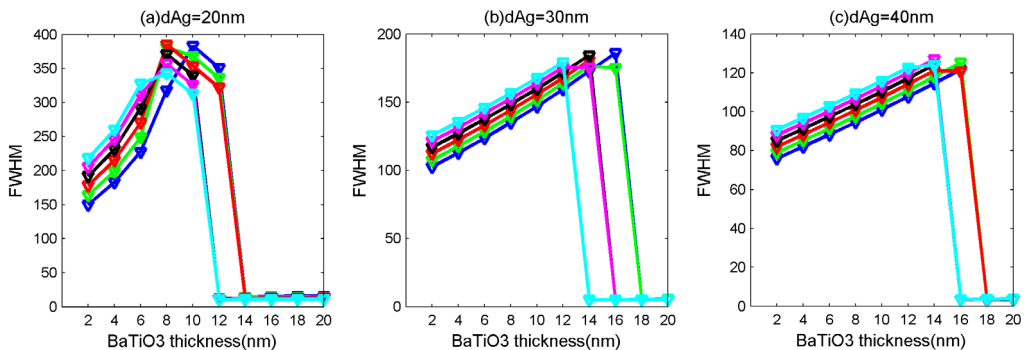

Fig. 2. FWHM of the proposed sensor for (a) 20, (b) 30, (c) 40, (d) 50, (e) 60, (f) 70, (g) 80, and (h) 90 nm Ag.
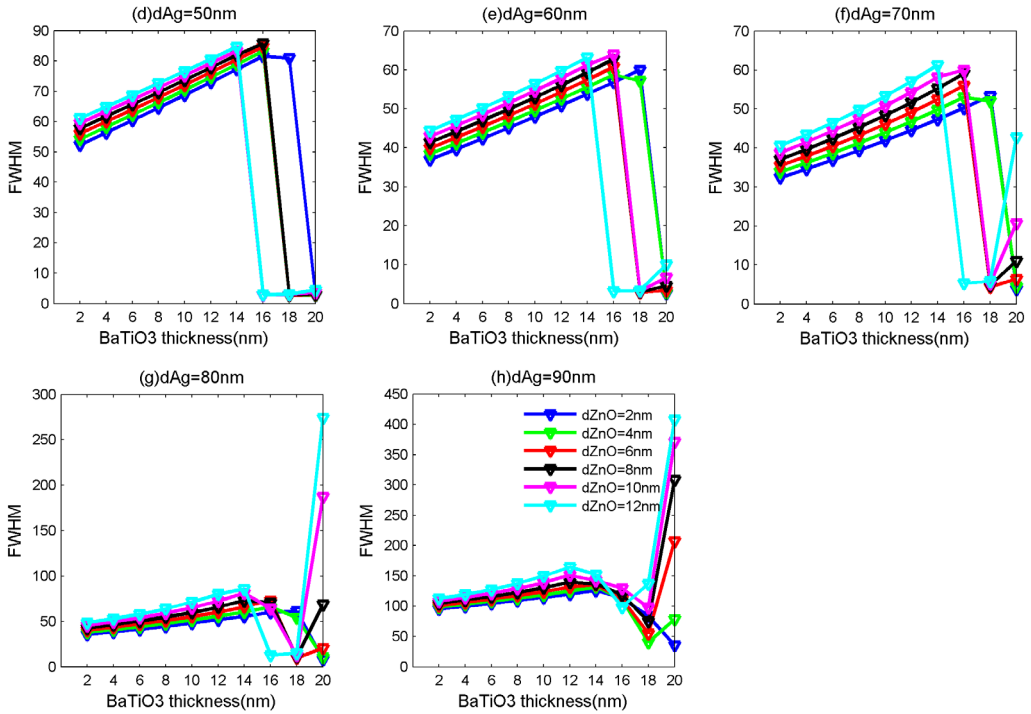
Fig. 2. Continiued.

tively. Figure 2 shows the FWHMs are lower for 50, 60, and 70 nm Ag than that for other thicknesses, and some of the FWHM values decrease sharply and are close to 0 for 12–20 nm thick $BaTiO_3$. The reason for the sudden drop of FWHM can be explained as follows: the resonance wavelengths of the reflected waveforms undergo redshift along with the increase in the thickness of $BaTiO_3$. Once the parts of a waveform are out of the scan wavelength range, the FWHM value cannot be captured. When the Ag thickness is between 30 and 80 nm, FWHM increases with the increase in the thickness of ZnO. For a fixed $BaTiO_3$ thickness, 2 nm ZnO shows the lowest FWHM value (see the solid blue line in Figs. 2(b)–(g)). In addition, the FWHM value increases generally with the increase of $BaTiO_3$ thickness, but it increases abnormally for 20 nm $BaTiO_3$, which means that the effect of SPR is not evident. Thus, only the range of 2–18 nm is considered for the optimization of $BaTiO_3$ thickness.

The thicknesses of the sensing layers are optimized to obtain the highest sensitivity, which is a critical parameter for the SPR sensor. According to literature [39], the sensitivity of the SPR sensor routinely increases with the increase in the thickness of $BaTiO_3$. Hence, two principles for optimization are identified: (1) $BaTiO_3$ should be as thick as possible, meaning high sensitivity. (2) FWHM has a reasonable value, indicating the integration of the reflected waveform. According to the mentioned principles, Table 1 lists the preferred thicknesses of Ag from 20 to 90 nm, $BaTiO_3$ from 2 to18 nm, and ZnO from 2 to12 nm. The corresponding fitting sensitivities are also calculated. Table 1

T a b l e 1. Preferred thicknesses of sensing layers and corresponding fitting sensitivities.

d_{Ag} [nm]	d_{ZnO} [nm]	d_{BaTiO3} [nm]	Fitting sensitivity [nm/(g·dL)]	d_{Ag} [nm]	d_{ZnO} [nm]	d_{BaTiO3} [nm]	Fitting sensitivity [nm/(g·dL)]
	2	12	7.9201		2	18	10.0581
	4	12	7.9997		4	18	9.8861
20	6	12	8.0492	60	6	16	9.4540
	8	10	7.6935		8	16	9.2924
	10	10	7.7241		10	16	9.1210
	12	10	7.7320		12	14	8.7739
	2	16	9.3206		2	18	10.0873
	4	16	9.2403		4	18	9.9126
30	6	14	8.8412	70	6	16	9.4793
	8	14	8.7592		8	16	9.3152
	10	14	8.6612		10	16	9.1418
	12	12	8.3314		12	14	8.7946
	2	16	9.5571		2	18	10.1052
	4	16	9.4433		4	18	9.9296
40	6	16	9.315	80	6	16	9.4964
	8	14	8.9342		8	16	9.3308
	10	14	8.8095		10	16	9.1568
	12	14	8.6732		12	14	8.8098
	2	18	10.0018		2	18	10.1186
	4	16	9.5505		4	18	9.9443
50	6	16	9.4068	90	6	18	9.7579
	8	16	9.2511		8	18	9.5622
	10	14	8.8871		10	18	9.3602
	12	14	8.7393		12	18	8.9379

shows that 18 nm $BaTiO_3$, 2 nm ZnO, and Ag from 50 to 90 nm demonstrate higher sensitivities that exceed 10 nm/(g·dL).

Moreover, the reflectivity of the reflected spectrum is considered for the optimization of Ag thickness. The minimum value of reflectance tells the maximum coupling of incident light with the SPW, and a lower minimum reflectivity indicates a stronger SPR effect. Figure 3 shows the reflected spectra are plotted using 18 nm thickness of $BaTiO_3$, 2 nm thickness of ZnO, and 50, 60, 70, 80, and 90 nm thickness of Ag. The minimum reflectivity increases gradually with the increase in Ag thickness, *i.e.*, close to 0 for 50 nm Ag (Fig. 3(a)), about 0.15 a.u. for 60 nm Ag (Fig. 3(b)), about 0.45 a.u. for 80 nm Ag (Fig. 3(c)), about 0.7 a.u. for 80 nm Ag (Fig. 3(d)), and greater than 0.8 a.u. for 90 nm Ag (Fig. 3(e)). Therefore, the curve tendency shows 80 and 90 nm as well as thicker than 90 nm Ag are not suitable for the optimal thickness of Ag due to the exorbitant minimum reflectivity.
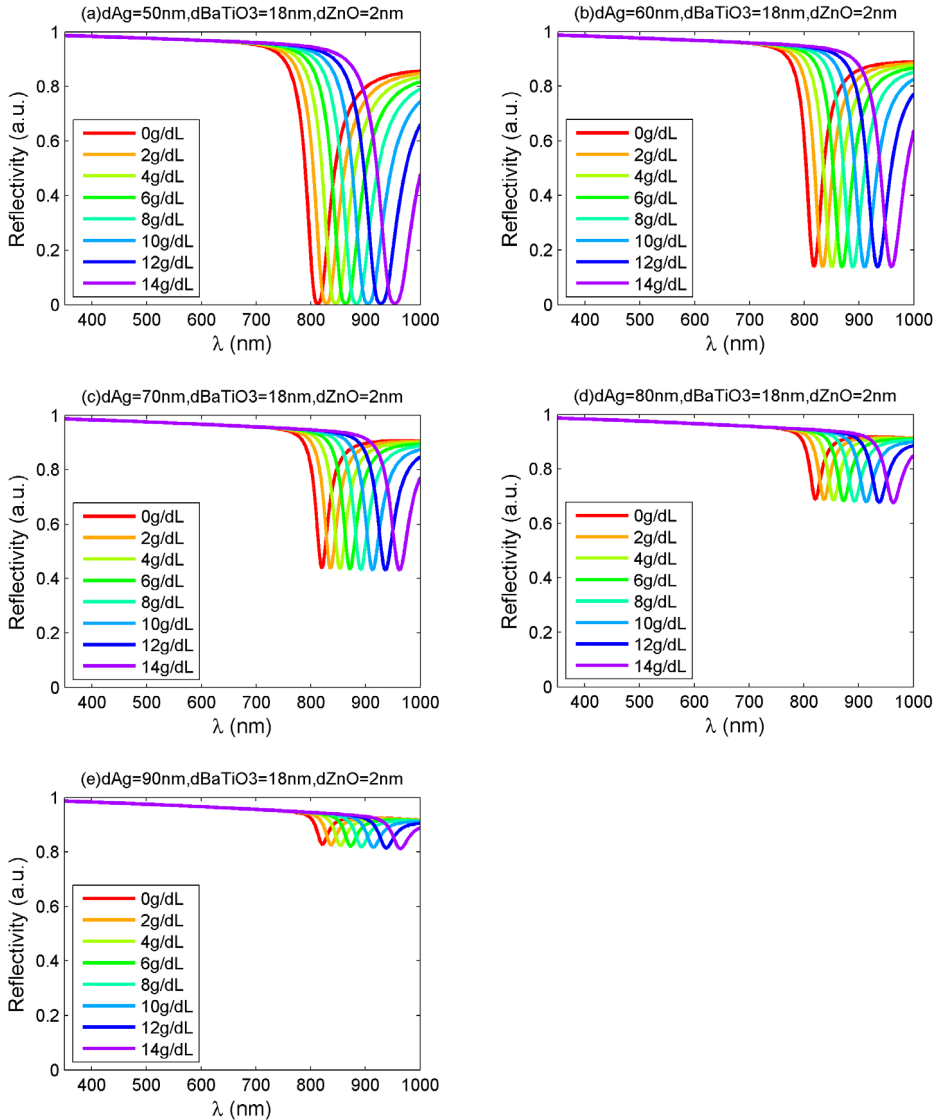
Fig. 3. Reflectivity at 18 nm BaTiO$_3$, 2 nm ZnO, and (a) 50, (b) 60, (c) 70, (d) 80, and (e) 90 nm Ag.

Furthermore, the FOM of the proposed SPR sensor is used to optimize Ag thickness, which is related to concentration sensitivity S_C and DA. Table 2 and Fig. 4 show the FOM comparison for different Ag thicknesses. On keeping the Ag thickness unchanged, the FOM value increases gradually with the increase in Hb concentration. For Hb concentration variation from 0 to 14 g/dL, 70 nm Ag exhibits the highest FOM value from 0.2170 dL/g for 2 g/dL to 0.2415 dL/g for 14 g/dL, hence serving as the optimal thickness of Ag. Figure 4 also shows that the concentration sensitivities

T a b l e 2. FOM comparison for different Ag thicknesses.

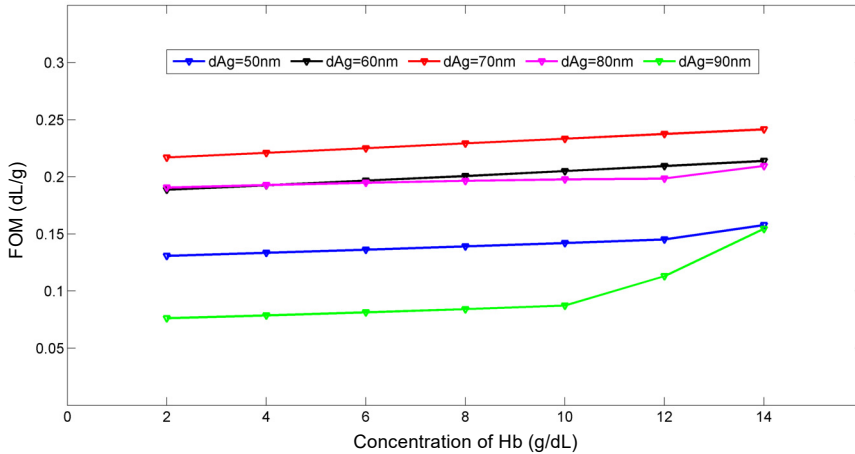| Ag thickness [nm]	C_{Hb} [g/dL]	FWHM [nm]	DA [nm^{-1}]	λ_{res} [nm]	$\Delta\lambda_{res}$ [nm]	$S_C = \Delta\lambda_{res}/\Delta C_{Hb}$ [nm/(g·dL)]	FOM = S_C/FWHM [dL/g]
	0	57.24	0.0175	812.37	–	–	–
	2	60.12	0.0166	828.1	15.73	7.865	0.1308
	4	63.3	0.0158	845	16.9	8.45	0.1335
	6	66.84	0.0150	863.21	18.21	9.105	0.1362
50	8	70.79	0.0141	882.91	19.7	9.85	0.1391
	10	75.23	0.0133	904.28	21.37	10.685	0.1420
	12	80.26	0.0125	927.59	23.31	11.655	0.1452
	14	80.94	0.0124	953.13	25.54	12.77	0.1578
	0	39.95	0.0250	817.63	–	–	–
	2	41.94	0.0238	833.47	15.84	7.92	0.1888
	4	44.14	0.0227	850.47	17	8.5	0.1926
	6	46.59	0.0215	868.8	18.33	9.165	0.1967
60	8	49.33	0.0203	888.6	19.8	9.9	0.2007
	10	52.42	0.0191	910.09	21.49	10.745	0.2050
	12	55.94	0.0179	933.52	23.43	11.715	0.2094
	14	59.97	0.0167	959.18	25.66	12.83	0.2139
	0	34.84	0.0287	819.93	–	–	–
	2	36.62	0.0273	835.82	15.89	7.945	0.2170
	4	38.6	0.0259	852.88	17.06	8.53	0.2210
	6	40.82	0.0245	871.25	18.37	9.185	0.2250
70	8	43.32	0.0231	891.12	19.87	9.935	0.2293
	10	46.18	0.0217	912.67	21.55	10.775	0.2333
	12	49.46	0.0202	936.16	23.49	11.745	0.2375
	14	53.28	0.0188	961.89	25.73	12.865	0.2415
	0	39.51	0.0253	820.97	–	–	–
	2	41.76	0.0239	836.89	15.92	7.96	0.1906
	4	44.32	0.0226	853.98	17.09	8.545	0.1928
	6	47.25	0.0212	872.39	18.41	9.205	0.1948
80	8	50.63	0.0198	892.29	19.9	9.95	0.1965
	10	54.58	0.0183	913.88	21.59	10.795	0.1978
	12	59.3	0.0169	937.41	23.53	11.765	0.1984
	14	61.54	0.0162	963.18	25.77	12.885	0.2094
	0	100.94	0.0099	821.52	–	–	–
	2	104.6	0.0096	837.46	15.94	7.97	0.0762
	4	108.65	0.0092	854.57	17.11	8.555	0.0787
	6	113.2	0.0088	873	18.43	9.215	0.0814
90	8	118.36	0.0084	892.93	19.93	9.965	0.0842
	10	123.84	0.0081	914.55	21.62	10.81	0.0873
	12	104.27	0.0096	938.11	23.56	11.78	0.1130
	14	83.53	0.0120	963.92	25.81	12.905	0.1545

Fig. 4. FOM of the proposed sensor with different Ag thicknesses.

increase with the increment in Ag thickness varying from 50 to 90 nm, whereas FOM values increase with the Ag thickness from 50 to 70 nm (blue, black, and red lines) and subsequently decrease after 80 nm (purple and green lines), moving down from the highest FOM value. This behavior is due to the wider FWHM for Ag of greater than 80 nm thickness increasing the denominator in FOM equation and causing the FOM to decrease.

As a result, the optimal thicknesses of sensing layers are obtained: 70 nm Ag, 2 nm ZnO, and 18 nm $BaTiO_3$.

4.2. Sensitivity enhancement

Now, the more important thing is how much $BaTiO_3$ enhances the sensitivity of proposed sensor, which is the focus of this paper. As for the item, the sensitivity enhancements by $BaTiO_3$ for Hb concentration and refractive index (RI) were analyzed, as shown in Table 3. Incorporating 18 nm $BaTiO_3$ in the configuration results in a maximum sensitivity enhancement of 30.74% for concentration and 26.67% for RI. The table also exhibits that a higher Hb concentration helps improve sensitivities, *i.e.*, 7.945 nm/(g·dL) and 3149 nm/RIU for 2 g/dL, and 12.865 nm/(g·dL) and 5173 nm/RIU for 14 g/dL at 18 nm $BaTiO_3$.

Again, the fitting curves for RI sensitivity and S_C are plotted to investigate further the extent to which $BaTiO_3$ affects sensitivity. Figure 5(a) shows the fitted RI sensitivity S_n for 0 nm $BaTiO_3$ is 3190 nm/RIU along with fitness of 0.9934 and nonlinear error of 0.7%, whereas for 18 nm $BaTiO_3$, the data are 4023 nm/RIU, 0.9931 and 0.65%, respectively. Hence, adding 18 nm $BaTiO_3$ leads to a mean RI sensitivity enhancement of 26.11% (higher than 23.68% in [25]) and helps reduce nonlinear error. Figure 5(b) provides the influence of 18 nm $BaTiO_3$ on the S_C. The fitted S_C for 0 and 18 nm $BaTiO_3$ are 7.7513 and 10.0873 nm/(g·dL) (corresponding resolution is 0.0099 g/dL), respec-

T a b l e 3. Sensitivity enhancement by BaTiO$_3$ with 70 nm Ag and 2 nm ZnO.

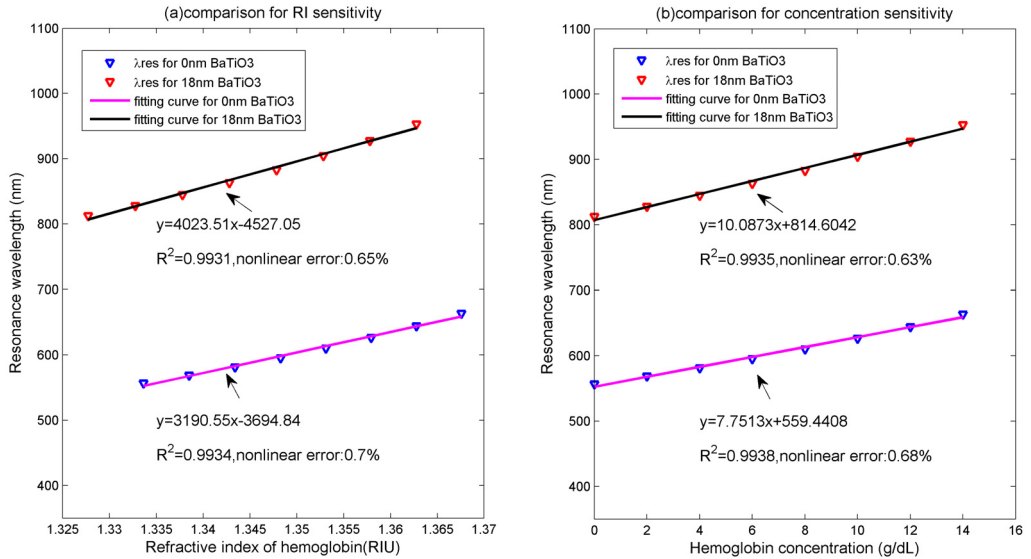| BaTiO$_3$ thickness [nm]	C_{Hb} [g/dL]	λ_{res} [nm]	$\Delta\lambda_{res}$ [nm]	$S_C = \Delta\lambda_{res}/\Delta C_{Hb}$ [nm/(g·dL)]	Concentration sensitivity enhancement [%]	n_{Hb} [RIU]	$S_n = \Delta\lambda_{res}/\Delta n_{Hb}$ [nm/RIU]	RI sensitivity enhancement [%]
	0	563.45	–	–	–	1.3334	–	–
	2	575.73	12.28	6.14	–	1.3383	2511	–
	4	588.88	13.15	6.575	–	1.3431	2694	–
	6	603.03	14.15	7.075	–	1.3480	2905	–
0	8	618.3	15.27	7.635	–	1.3529	3142	–
	10	634.85	16.55	8.275	–	1.3577	3414	–
	12	652.84	17.99	8.995	–	1.3625	3721	–
	14	672.52	19.68	9.84	–	1.3674	4084	–
	0	819.93	–	–	–	1.3276	–	–
	2	835.82	15.89	7.945	29.40	1.3326	3149	25.38
	4	852.88	17.06	8.53	29.73	1.3377	3387	25.73
	6	871.25	18.37	9.185	29.82	1.3427	3655	25.81
18	8	891.12	19.87	9.935	30.12	1.3477	3962	26.10
	10	912.67	21.55	10.775	30.21	1.3527	4308	26.18
	12	936.16	23.49	11.745	30.57	1.3577	4709	26.53
	14	961.89	25.73	12.865	30.74	1.3627	5173	26.67

Fig. 5. Comparison for (a) RI sensitivity, and (b) S_C enhanced by BaTiO$_3$.

tively, resulting in a mean S_C enhancement of 30.14%. The nonlinear error has been reduced, *i.e.*, 0.68% for 0 nm BaTiO$_3$ and 0.63% for 18 nm BaTiO$_3$.

As mentioned above, BaTiO$_3$ can improve the sensitivity of the proposed sensor. Here, the sensitivity enhancement effect is viewed from the reflected spectra. Figure 6 shows the reflected spectra (see the right area in the figure) for the proposed sensor with 18 nm thick BaTiO$_3$ are compared with that (see the left area in the figure) without BaTiO$_3$. Corresponding to the same variation in Hb concentration (ΔC_{Hb}), the shifts in the resonance wavelength ($\Delta \lambda_{res}$) of the reflected spectra clearly increase after adding BaTiO$_3$. The S_C of the proposed sensor is enhanced by BaTiO$_3$. In addition, although
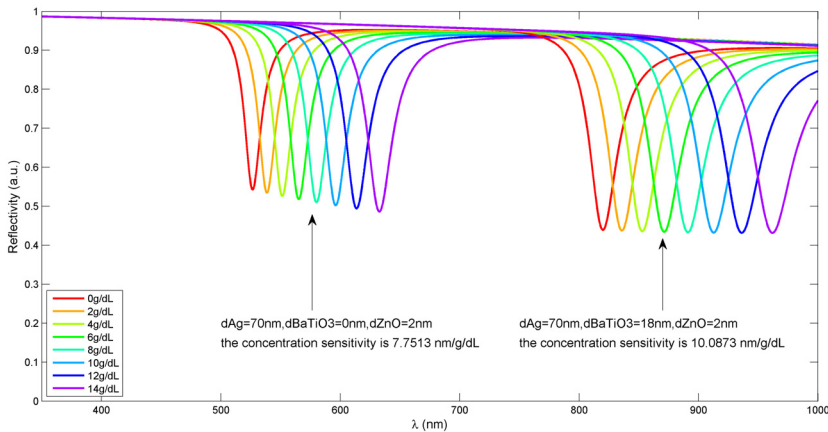

Fig. 6. Comparison of spectrum of optical fiber SPR sensor with 0 and 18 nm BaTiO$_3$.

T a b l e 4. Comparison for RI sensitivity enhancement by BaTiO₃ with existing wavelength interrogation-based optical fiber SPR sensor.

Sensor structure	RI range	RI sensitivity [nm/RIU]	RI sensitivity enhancement by BaTiO$_3$ [%]	Reference
Fiber/Au	1.3332–1.3710	2280		[25]
Fiber/Au/BaTiO$_3$	1.3332–1.3710	2820	23.68	
Fiber/Ag/ZnO	1.3334–1.3674	3190		This work
Fiber/Ag/BaTiO$_3$/ZnO	1.3276–1.3627	4023	26.11	

T a b l e 5. Comparison for the sensitivity and resolution with existing SPR sensor for Hb concentration detection.

Sensor structure	Interrogation mode	Hb concentration range	Wavelength	RI sensitivity concentration sensitivity	Resolution	Reference
Prism/Ag/BaTiO$_3$/antimonene	Angle	0–140 g/L	632.8 nm	303.83°/RIU 0.045°/gL^{-1}	0.021 g/L	[40]
Fiber/Ag/BaTiO$_3$/ZnO	Wavelength	0–14 g/dL	350–1100 nm	4023 nm/RIU 10.0873 nm/(g·dL)	0.0099 g/dL (= 0.099 g/L)	This work

the sensitivity is improved, the waveforms of reflected spectra are widened, leading to the increments in FWHM shown in Table 3.

Finally, the optical fiber SPR sensor presented in this paper is compared with existing literature, as shown in Tables 4 and 5. The data in Table 4 exhibit the SPR sensor proposed in this paper has better sensitivity enhancement by $BaTiO_3$ than existing wavelength interrogation-based optical fiber SPR sensor. However, compared with the SPR sensor based on angular interrogation, a lower Hb concentration detection resolution for proposed SPR sensor is observed, as shown in Table 5.

5. Conclusion

In this paper, a wavelength interrogation-based optical fiber SPR sensor for Hb concentration using Ag, $BaTiO_3$, and ZnO is proposed. With light wavelength ranging from 350 to 1000 nm, the optimal thicknesses of sensing layers are obtained: 70 nm Ag, 18 nm $BaTiO_3$, and 2 nm ZnO for 0–14 g/dL Hb concentration. Then sensitivity enhancement by $BaTiO_3$ is observed from fitting sensitivity. The simulation results show that using 18 nm $BaTiO_3$ can provide a fitted RI sensitivity of 4023 nm/RIU and an S_C of 10.0873 nm/(g·dL), which indicate the corresponding sensitivity enhancements of 26.11% and 30.14%, respectively. Our results are compared with existing wavelength interrogation-based optical fiber SPR sensor, demonstrating the RI sensitivity enhancement of 26.11% is higher than that of 23.68% in [25]. Hence, the proposed sensor has a reasonable configuration, the optimization approach is correct, and a good effect for sensitivity enhancement is obtained.

Enhanced as the sensitivity is, the proposed sensor provides a lower Hb concentration detection resolution than reported SPR sensor that works in angular interrogation mode [40]. This problem can be solved by further optimizing the sensor configuration and using nanomaterials with better optical properties.

In addition, different from angular interrogation-based sensor, FWHM is a remarkable parameter for wavelength interrogation-based sensor in identifying the integrity of reflected waveform influenced by wavelength shift. Furthermore, using $BaTiO_3$ causes the wavelength shift of the reflected spectra, which is conducive to the realization of the multichannel detection technique for Hb concentration.

As mentioned above, the proposed optical fiber SPR sensor is suitable for detecting Hb concentration and more convenient for applications than prism-based and angular interrogation-based SPR sensor. This paper will provide others some consideration for optimization approach and performance improvement of wavelength interrogation -based optical fiber SPR sensor.

References

[1] MORENO Y., SONG Q., XING Z., SUN Y., YAN Z., *Hybrid tilted fiber gratings-based surface plasmon resonance sensor and its application for hemoglobin detection*, Chinese Optics Letters **18**(10), 2020: 100601.

[2] FRIEBEL M., MEINKE M., *Model function to calculate the refractive index of native hemoglobin in the wavelength range of 250–1100 nm dependent on concentration*, Applied Optics **45**(12), 2006: 2838-2842. https://doi.org/10.1364/AO.45.002838

[3] ZHERNOVAYA O., SYDORUK O., TUCHIN V., DOUPLIK A., *The refractive index of human hemoglobin in the visible range*, Physics in Medicine and Biology **56**(13), 2011: 4013-4021. https://doi.org/10.1088/0031-9155/56/13/017

[4] BARER R., *Refractometry and interferometry of living cells*, Journal of the Optical Society of America **47**(6), 1957: 545-556. https://doi.org/10.1364/JOSA.47.000545

[5] SHARMA A.K., JHA R., PATTANAIK H.S., *Design considerations for surface plasmon resonance based detection of human blood group in near infrared*, Journal of Applied Physics **107**(3), 2010: 034701. https://doi.org/10.1063/1.3298503

[6] NGUYEN T.T., BEA S.O., KIN D.M., YOON W.J., PARK J.-W., AN S.S.A., JU H., *A regenerative label-free fiber optic sensor using surface plasmon resonance for clinical diagnosis of fibrinogen*, International Journal of Nanomedicine **10**, 2015: 155-163. https://doi.org/10.2147/ijn.s88963

[7] LIEDBERG B., NYLANDER C., LUNSTRÖM I., *Surface plasmon resonance for gas detection and biosensing*, Sensors and Actuators **4**, 1983: 299-304. https://doi.org/10.1016/0250-6874(83)85036-7

[8] BRAHMACHARI K., RAY M., *Modelling and performance analysis of a plasmonic biosensor comprising of silicon and chalcogenide materials for detecting refractive index variations of hemoglobin in near infrared*, Optik **127**(7), 2016: 3517-3522. https://doi.org/10.1016/j.ijleo.2015.12.148

[9] HEIDARZADEH H., *Analysis and simulation of a plasmonic biosensor for hemoglobin concentration detection using noble metal nano-particles resonances*, Optics Communications **459**, 2019: 124940. https://doi.org/10.1016/j.optcom.2019.124940

[10] MOHANTY G., SAHOO B.K., *Effect of III-V nitrides on performance of graphene based SPR biosensor for detection of hemoglobin in human blood sample: A comparative analysis*, Current Applied Physics **16**(12), 2016, 1607-1613. https://doi.org/10.1016/j.cap.2016.09.006

[11] TENG C., LI M., CHENG Y., PENG H., DENG S., DENG H., YUAN L., CHEN M., *Investigation of U-shape tapered plastic optical fibers based surface plasmon resonance sensor for RI sensing*, Optik **251**, 2022: 168461. https://doi.org/10.1016/j.ijleo.2021.168461

[12] JAIN S., PALIWAL A., GUPTA V., TOMAR M., *Smartphone integrated handheld long range surface plasmon resonance based fiber-optic biosensor with tunable SiO_2 sensing matrix*, Biosensors and Bioelectronics **201**, 2022: 113919. https://doi.org/10.1016/j.bios.2021.113919

[13] DENG Y., LI M., CAO W., WANG M., HAO H., XIA W., SU F., *Fiber optic coupled surface plasmon resonance sensor based $Ag-TiO_2$ films for hydrogen detection*, Optical Fiber Technology **65**, 2021: 102616. https://doi.org/10.1016/j.yofte.2021.102616

[14] SHOJI A., NAKAJIMA M., MORIOKA K., FUJIMORI E., UMEMURA T., YANAGIDA A., HEMMI A., UCHIYAMA K., NAKAJIMA H., *Development of a surface plasmon resonance sensor using an optical fiber prepared by electroless displacement gold plating and its application to immunoassay*, Talanta **240**, 2022: 123162. https://doi.org/10.1016/j.talanta.2021.123162

[15] WANG Y., XU J., NING T., LIU L., ZHENG J., WANG J., PEI L., ZHANG J., YOU H., *Research on fiber-optic magnetic field sensor based on surface plasmon resonance*, Optik **251**, 2022: 168346. https://doi.org/10.1016/j.ijleo.2021.168346

[16] DUBEY S.K., KUMAR A., KUMAR A., PATHAK A., SRIVASTAVA S.K., *A study of highly sensitive D-shaped optical fiber surface plasmon resonance based refractive index sensor using grating structures of Ag-TiO$_2$ and Ag-SnO$_2$*, Optik **252**, 2022: 168527. https://doi.org/10.1016/j.ijleo.2021.168527

[17] HOMOLA J., *Optical fiber sensor based on surface plasmon excitation*, Sensors and Actuators B: Chemical **29**(1-3), 1995: 401-405. https://doi.org/10.1016/0925-4005(95)01714-3

[18] LIN W.B., JAFFREZIC-RENAULT N., GAGNAIRE A., GAGNAIRE H., *The effects of polarization of the incident light-modeling and analysis of a SPR multimode optical fiber sensor*, Sensors and Actuators A: Physical **84**(3), 2000: 198-204. https://doi.org/10.1016/S0924-4247(00)00345-9

[19] SHARMA A.K., GUPTA B.D., *Absorption-based fiber optic surface plasmon resonance sensor: a theoretical evaluation*, Sensors and Actuators B: Chemical **100**(3), 2004: 423-431. https://doi.org/10.1016/j.snb.2004.02.013

[20] SHARMA A.K., *Plasmonic biosensor for detection of hemoglobin concentration in human blood: Design considerations*, Journal of Applied Physics **114**(4), 2013: 044701. https://doi.org/10.1063/1.4816272

[21] LUO M., WANG Q., *A reflective optical fiber SPR sensor with surface modified hemoglobin for dissolved oxygen detection*, Alexandria Engineering Journal **60**(4), 2021: 4115-4120. https://doi.org/10.1016/j.aej.2020.12.041

[22] SRIVASTAVA S.K., ARORA V., SAPRA S., GUPTA B.D., *Localized surface plasmon resonance-based fiber optic U-shaped biosensor for the detection of blood glucose*, Plasmonics **7**, 2012: 261-268. https://doi.org/10.1007/s11468-011-9302-8

[23] RANI M., SHUKLA S., SHARMA N.K., SAJAL V., *Theoretical study of nanocomposites based fiber optic SPR sensor*, Optics Communications **313**, 2014: 303-314. https://doi.org/10.1016/j.optcom.2013.10.048

[24] SUN P., WANG M., LIU L., JIAO L., DU W., XIA F., LIU M., KONG W., DONG L., YUN M., *Sensitivity enhancement of surface plasmon resonance biosensor based on graphene and barium titanate layers*, Applied Surface Science **475**, 2019, 342-347. https://doi.org/10.1016/j.apsusc.2018.12.283

[25] WANG Q., NIU L.-Y., JING J.-Y., ZHAO W.-M., *Barium titanate film based fiber optic surface plasmon sensor with high sensitivity*, Optics & Laser Technology **124**, 2020: 105899. https://doi.org/10.1016/j.optlastec.2019.105899

[26] WAN Q., LI Q.H., CHEN Y.J., WANG T.H., HE X.L., LI J.P., LIN C.L., *Fabrication and ethanol sensing characteristics of ZnO nanowire gas sensors*, Applied Physics Letters **84**(18), 2004: 3554-3656. https://doi.org/10.1063/1.1738932

[27] WANG J.X., SUN X.W., WEI A., LEI Y., CAI X.P., LI C.M., DONG Z.L., *Zinc oxide nanocomb biosensor for glucose detection*, Applied Physics Letters **88**(23), 2006: 233106. https://doi.org/10.1063/1.2210078

[28] GUPTA S.K., JOSHI A., KAUR M., *Development of gas sensors using ZnO nanostructures*, Journal of Chemical Sciences **122**, 2010: 57-62. https://doi.org/10.1007/s12039-010-0006-y

[29] DOSTALEK J., KASRY A., KNOLL W., *Long range surface plasmons for observation of biomolecular binding events at metallic surfaces*, Plasmonics **2**, 2007: 97-106. https://doi.org/10.1007/s11468-007-9037-8

[30] SHUKLA S., SHARMA N.K., SAJAL V., *Sensitivity enhancement of a surface plasmon resonance based fiber optic sensor using ZnO thin film: a theoretical study*, Sensors and Actuators B: Chemical **206**, 2015: 463-470. https://doi.org/10.1016/j.snb.2014.09.083

[31] NAYAK J.K., JHA R., *Numerical simulation on the performance analysis of a graphene-coated optical fiber plasmonic sensor at anti-crossing*, Applied Optics **56**(10), 2017: 3510-3517. https://doi.org/10.1364/AO.56.003510

[32] ORDAL M.A., LONG L.L., BELL R.J., BELL S.E., BELL R.R., ALEXANDER R.W., WARD C.A., *Optical properties of metals Al, Co, Cu, Au, Fe, Pb, Ni, Pd, Pt, Ag, Ti, and W in the infrared and far infrared*, Applied Optics **22**(7), 1983: 1099-1119. https://doi.org/10.1364/AO.22.001099

[33] WEMPLE S.H., DIDOMENICO M., CAMLIBEL I., *Dielectric and optical properties of melt-grown BaTiO$_3$*, Journal of Physics and Chemistry of Solids **29**(10), 1968: 1797-1803. https://doi.org/10.1016/0022-3697(68)90164-9

[34] SACHET E., LOSEGO M.D., GUSKE J., FRANZEN S., MARIA J.P., *Mid-infrared surface plasmon resonance in zinc oxide semiconductor thin films*, Applied Physics Letters **102**(5), 2013: 051111. https://doi.org/10.1063/1.4791700

[35] HSU L.-S., YEH C.S., KUO C.C., HUANG B.R., DHAR S., *Optical and transport properties of undoped and Al-, Ga- and In-doped ZnO thin films*, Journal of Optoelectronics and Advanced Materials **7**(6), 2005: 3039-3046.

[36] JIANG L.G., SUN P., *Models of the wavelength dependence for the index of refraction of water*, Chinese Journal of Spectroscopy Laboratory **19**(4), 2002: 554-556.

[37] SHARMA A.K., GUPTA B.D., *On the performance of different bimetallic combinations in surface plasmon resonance based fiber optic sensors*, Journal of Applied Physics **101**(9), 2007: 093111. https://doi.org/10.1063/1.2721779

[38] PRAHL S., *Optical Absorption of Hemoglobin*, Oregon Medical Laser Center, 1999. http://omlc.ogi.edu/spectra/hemoglobin

[39] SETAREH M., KAATUZIAN H., *Sensitivity enhancement of a surface plasmon resonance sensor using Blue Phosphorene/MoS$_2$ hetero-structure and barium titanate*, Superlattices and Microstructures **153**, 2021: 106867. https://doi.org/10.1016/j.spmi.2021.106867

[40] SINGH M.K., PAL S., VERMA A., DAS R., PRAJAPATI Y.K., *A nanolayered structure for sensitive detection of hemoglobin concentration using surface plasmon resonance*, Applied Physics A **127**, 2021: 832. https://doi.org/10.1007/s00339-021-04985-w